RESEARCH ARTICLE

ISSN: 2321-7758

ELECTRICAL, MAGNETIC AND OPTICAL PROPERTIES OF SYNTHETIC NANOFERRITES

M.S. SUBBA RAJU

Sr. Lecturer in Physics, Mrs.A.V.N.College, Visakhapatnam, Andhra Pradesh

ABSTRACT

Nanocomposites, a high performance material exhibit unusual property combinations and unique design possibilities. Electrical, Magnetic and Optical properties of Magnesium ion doped in Nickel-Zinc nanoferrites are studied, $Mg_x Zn_{0.2} Ni_{0.2} Fe_{2-x} O_4$ (where x=0.0, 0.2, 0.4) (MZN) reaction Nano crystalline ferrites were synthesized by sol-gel auto combustion method. The XRD characterization gives the particle size and it was calculated from XRD by Scherrer's formula. The X-ray diffraction pattern of all the samples provide the information about the particle size of synthesized samples were found to be decreases with the increase in Mg^{2+} concentration. Crystallite size was estimated and was found to lie in the range of 39 ± 4nm. The optical properties of synthesized samples were investigated from UV visible spectra. The magnetic measurement shows that the saturation magnetization and remanence magnetization decreases with the increase in the Magnesium content. Room temperature dielectric studies revealed low dielectric constant and low dielectric loss values. Resistivity values were enhanced with Mg doping up to a particular concentration.

Key Words: Nanoferrites-Magnesium doiping-Electical properties-Magnetic properties-Optical Properties

Introduction

The last few decades saw substantial development in the field of nano technology, particularly in physical sciences. The synthesis of nano crystalline spinel ferrites plays an important role in determining their physical properties at nano and sub nano levels. Ferrites have established their potential in several applications due to their remarkable electrical and magnetic properties, and also in magnetic resonance imaging (MRI) enhancement, magnetic high-density information storage etc[1]. The general formula of Spinel ferrites is MFe_2O_4 (where M = Mg^{2+}, Ni^{2+}, Cu^{2+}, Co^{2+}, Zn^{2+}) which is a class of hybrid functional materials. These are useful for designing of electrical and magnetic devices. The physical properties such as increase in DC resistivity, low dielectric losses and magnetization characteristics are due to the substitution of tetrahedral cations in the parent crystal structure. With the striking feature of "ferrimagnetism" nanocrystalline ferrites have attracted special attention of researchers in the field of electronic technology[2].Doping with Mg may improve the electromagnetic properties of Ni-Zn

ferrite samples. This is because of the fact that Mg containing composition may avoid the tendency of discontinuous grain growth[3].Hence an interesting aspect to study such types of system our current research work is the synthesis of $Mg_x Zn_{0.2} Ni_{0.2} Fe_{2-x} O_4$ (where x=0.0, 0.2, 0.4) nanoparticles by using sol-gel technique. Our main focus is to investigate the structural properties, electrical, optical and magnetic properties if MZN nanoferrite samples. The X-ray diffraction pattern and microstructure of prepared nanomaterials are discussed as function of Mg content.

Materials and Method

All the chemicals were purchased from Merck India, Sd fine chemicals and were used without extra purification (99.9% purity). Chemicals used in the synthesis were $(Ni(NO_3)_2.6H_2O)$, magnesium nitrate $(Mg(NO_3)_2.6H_2O)$, zinc nitrate $(Zn(NO_3)_2.6H_2O)$, ferric nitrate $(Fe(NO_3)_3.9H_2O)$ and citric acid $(C_6H_8O_7)$. The stoichiometric amounts of metal nitrates and citric acid were dissolved in double distilled water. Metal nitrate solutions were mixed with citric acid solution in 1:1 molar ratio of nitrate to citric acid. The pH of the solution was maintained at 7.0 using ammonia solution. Then the solution was heated at 100°C to transform into a thick gel. Thereafter, the gel ignited and burnt with glowing flints yielding loose ferrite powder. The as-burnt powder was granulated using 15% polyvinyl alcohol as a binder and was pressed to form pellets (10mm diameter) and toroidal rings (30mm outer diameter, 10mm inner diameter and 3mm thickness) by applying a pressure of 10 ton cm^{-2}. These specimens were pre-sintered at 700°C for 3h in a programmable conventional furnace to expel the binder and were then subjected to final sintering at 800°C for 3h using the above mentioned furnace at a heating rate of 5°C/min. The samples were furnace cooled.

Characterizations

$Mg_x Zn_{0.2} Ni_{0.2} Fe_{2-x} O_4$ (where x=0.0, 0.2, 0.4) formation was confirmed by the XRD (Philips) with Cu Kα (λ=1.5405Å) results. Furthermore UV-Vis-NIR spectrophotometer at room temperature was used to study the UV–Vis absorption spectra. Magnetic characterizations were measured using a vibrating sample magnetometer (VSM) that allows measures in range between 77 - 650 K in magnetic fields until 10 kOe and parameters like specific saturation magnitization (Ms), corecive force (Hc) and remanence (Mr) were evaluated. Electrical properties such as permittivity and loss tangent were determined using a vector network analyzer equipment ROHDE & SCHWARZ model ZVB14.

Results and Discussion

Structural Characterization

The X-Ray Diffraction pattern for the sample $Mg_x Zn_{0.2} Ni_{0.2} Fe_{2-x} O_4$ (where x=0.0, 0.2, 0.4) is shown in Figure 1. This diffraction line provides a clear evidence for the formation of ferrite phase in all the samples. The experimental results revealed that the lattice parameter, X-ray density of the prepared ferrite samples, increases with increase in Mg-substituted concentration and the grain size is also in the nm range only. The broad XRD line indicates that the ferrite particles are of nano size. The average crystallite size for each composition was calculated from the full width at half maximum intensity for (311) plain using Scherrer's formula (equation 1)[4]. The values of the lattice parameter were determined by using the following equation.

$$a = \frac{d}{\sqrt{h^2+k^2+l^2}} \text{ ....(1)}$$

Where, h, k, l are miller indices. The values of the particle size and lattice constant as deduced from the X-Ray Diffraction are given in Table 1.
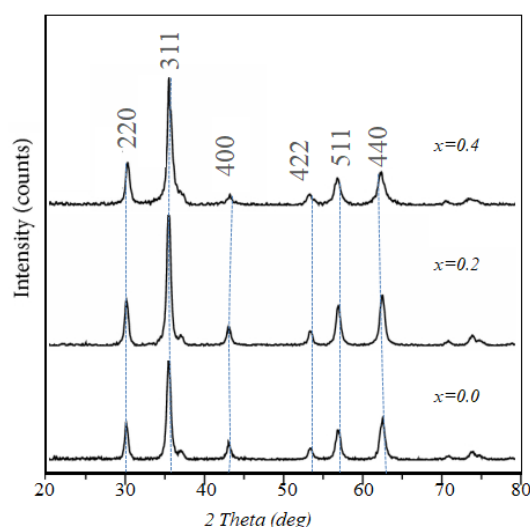
Figure 1. X-ray Diffraction Pattern for $Mg_x Zn_{0.2} Ni_{0.2} Fe_{2-x} O_4$ (where x=0.0, 0.2, 0.4)

Table 1. Magnetization at an applied field of 20 kOe for the samples $Mg_x Zn_{0.2} Ni_{0.2} Fe_{2-x} O_4$ (where x=0.0, 0.2, 0.4)

x	Composition	Å	Particle Size (nm)	M_{Max} (emu/g)	X-ray density (dx)
0	$Mg_0 Zn_{0.2} Ni_{0.2} Fe_2 O_4$	8.7023	40.25	12.57	4.319
0.2	$Mg_{0.2} Zn_{0.2} Ni_{0.2} Fe_{1.8} O_4$	8.6945	39.87	11.37	4.329
0.4	$Mg_{0.4} Zn_{0.2} Ni_{0.2} Fe_{1.6} O_4$	8.6342	38.24	9.67	4.553

In the present investigation, The bulk value of the lattice constant for $Mg_{0.4} Zn_{0.2} Ni_{0.2} Fe_{1.6}O_4$ reported as 8.6342Å and it was observed that decrease in the lattice constant. A similar decrease in the lattice constant was reported by Arulmurugan et al.(2008)[v]. This decrease in the lattice constant may be due to change in the cation distribution between A site and B site. in the nano regime[vi]. However there is an increase in the lattice constant with the increase in the Mg content. This increase in the lattice constant is due to larger ionic radii of the Mg^{2+} (0.65 Å) as compared to Fe^{3+} (0.63Å) ions. The intensities of the planes (220) and (440) are more sensitive to any change in cation on tetrahedral A sites and octahedral B sites respectively. Mg^{2+}ions and Zn^{2+} ions have chemical affinity towards tetrahedral A sites. Mean while Mg^{2+} and Fe^{3+} ions have, preferences for both tetrahedral A sites and octahedral B sites respectively. Since the X-Ray scattering factor for Mg^{2+}ion is significantly high as compared to those of the other cations, the intensities of the (220) plane and (440) plane increases with increasing Mg^{2+}ion concentration. This shows that Mg^{2+}ions occupy tetrahedral A sites and octahedral B sites in the nano dimension against their chemical preference for A site as observed in bulk samples. Hence there is a small increase in the intensities of (220) and (440) plane. The occupation of Mg^{2+}ion on the octahedral B site forces some of the Fe^{3+} ions to migrate from B site to A site. Hence there is a deviation in the cation distribution from normal in the Nano dimension. The average crystallite size of the prepared nanoferrite samples was in the ranges from 39-40 nm for different doping levels of the Mg^{+2} ions (table 1). The XRD pattern perfectly matches with the standard pattern with JCPDS reference code 00-24-157. X-ray density values of the Ni-Zn nanoferrites were increased with increasing the Mg concentration because molecular weight of the samples increases with increasing the Ni composition. It is noted that X-ray density of each sample (d_x).

Electrical Properties

The DC electrical conductivity of the prepared samples was measured by two-probe method in the temperature range from 473 K to 873 K. The ferrite sample is pressed into circular pellets. The measurements were recorded in the steps of 10 K.

The temperature dependence of the prepared ferrites conductivity is plotted in accordance with the following Arrhenius type equation:

$$\log \sigma = log\sigma_o - \frac{E_a}{K_B T} \quad ....(2)$$

where σ is the conductivity, σ_o is the conductivity at absolute temperature, K_B is Boltzmann's constant, and T is the temperature. The phenomenon of phase transition, cation migration, cation reordering, the presence of impurities, and magnetotransport effects are considered to be responsible for the temperature dependence on the electrical conductivity of the prepared ferrite samples.

The variations of the electrical conductivity (log σT) with inverse of temperature (1000/T) were shown in Figure 2. The conductivity of the ferrite samples increases with increasing the temperature. That is, temperature increases and resistivity of the ferrites was decreased, indicating the semiconducting behaviour. All the plots (except pure lithium ferrites) of electrical conductivity (log σT) versus (1000/T) yield a change in slope at a particular temperature. This change in slope occurs while crossing the Curie temperature (the temperature at which the ferromagnetic material changed to paramagnetic). The discontinuity at the Curie temperature was attributed to the magnetic

M.S. SUBBA RAJU

transition from well-ordered ferromagnetic state to disordered paramagnetic state which involves different activation energies. The values of the electrical resistivity and thermal activation energies of the prepared samples at ferromagnetic region and paramagnetic region were given in Table 2. It is observed that the activation energy in the ferromagnetic region is smaller than the paramagnetic region; this is due to the effect of spin disordering.
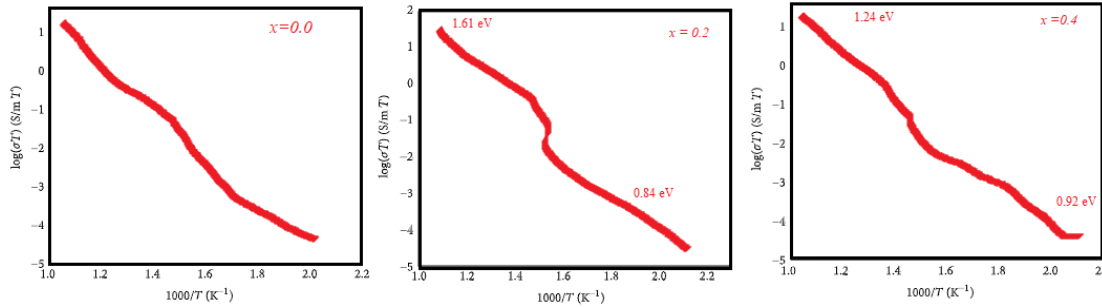
Figure 2: Arrhenius plots for electrical conductivities of $Mg_x Zn_{0.2} Ni_{0.2} Fe_{2-x} O_4$ (where x=0.0, 0.2, 0.4) nanoferrites.

Table 2: The variation of DC electrical resistivity with Mg composition in the Ni-Zn ferrites

x	Composition	Resistivity (Ω-cm)	Curie temp. (°C)	E_a in paramagnetic region (eV)	E_a in Ferromagnetic region (eV)
0	$Mg_0 Zn_{0.2} Ni_{0.2} Fe_2 O_4$	8.27×10^7	—	—	—
0.02	$Mg_{0.2} Zn_{0.2} Ni_{0.2} Fe_{1.8} O_4$	8.19×10^7	560	1.37	0.79
0.4	$Mg_{0.4} Zn_{0.2} Ni_{0.2} Fe_{1.6} O_4$	6.31×107	550	1.31	0.92

The variation of DC electrical resistivity at 550 and 560°C with Mg composition in the Ni-Zn ferrites is given in Table 2. The DC resistivity of the all the samples was observed to be in the range 8.27×10^7 to $6.31 \times 10^7 \times 108$ Ω-cm. Compositionally decrease in the DC resistivity of Ni-Zn ferrites with increasing the Mg concentration was observed. The overall higher values of resistivity obtained for the ferrites can be attributed to the small grain size and better compositional stoichiometry with reduced Fe^{+2} formation as a result of low temperature processing by the citrate gel method[vii].

Optical Properties

Traditionally, the optical properties of nanoferrites have long been extensively employed for amazing coloring effects glasses and paints. Due to awareness of renewable solar energy worldwide in the 1970s, researchers worked a lot on nanoparticle optics. High level of accuracy of models of optical properties is required in designing optical coatings. Application of nanoparticle based coatings can be further be optimized by making calculative changes in dimensional parameters. Different situations demand different classes of models due to complexity of optics. The optical properties of $Mg_x Zn_{0.2} Ni_{0.2} Fe_{2-x} O_4$ (where x=0.0, 0.2, 0.4) nanoparticles were studied using a Elico made-UV-visible spectrophotometer ranging from 200 to 800 nm. Figure 3 shows that the compositions at different concentrations exhibited spectra in the visible range. The absorption peaks are observed at 334nm, 336nm,340 nm and wavelength peaks are shifted. The UV visible indicates that sintering temperature and composition of the sample has the best influence on the optical property. The Kubelka–Munk model was used to compute the optical band gap energy (Eg). The band gap energy was calculated using a plot of $(ahv)^2$ vs. photon energy (hv), which is also called the Tauc plot, of the $Mg_x Zn_{0.2} Ni_{0.2} Fe_{2-x} O_4$ (where x=0.0, 0.2, 0.4) nanoparticles (Figure 4). It was observed that E_g= 3.60 ev for x=0.4 , E_g= 3.80 ev for x=0.2 E_g=3.97 eV for x=0.0. The band gap of the samples was found to vary from 3.5 eV - 3.9 eV with the variation in magnesium concentration . Thus, the estimated value of band gap decreases with the increase in

M.S. SUBBA RAJU

magnesium concentration. This may have arisen due to the additional sub-band gap energy levels induced due to the introduction of the magnesium. Hence, by introducing magnesium in nickel-zinc ferrite the absorption spectra and hence the band gap can be tuned. The concentration of the magnesium can be used to engineer the band gap for specific applications.
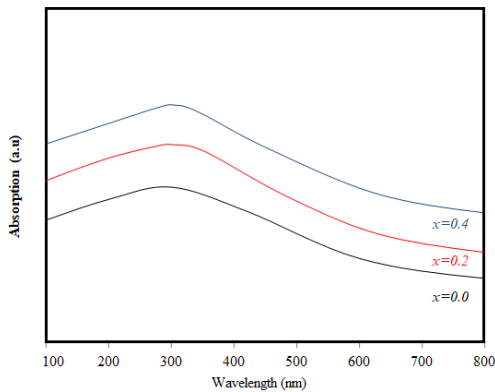
Figure 3. Absorption spectra for $Mg_x Zn_{0.2} Ni_{0.2} Fe_{2-x} O_4$ (where x=0.0, 0.2, 0.4) nanoferrites
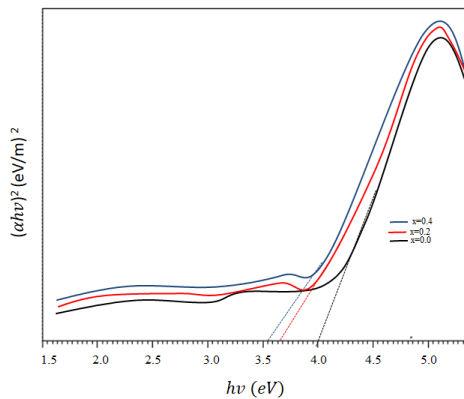
Figure 4:Plot of $(\alpha h v)^2$ versus hv for $Mg_x Zn_{0.2} Ni_{0.2} Fe_{2-x} O_4$ (where x=0.0, 0.2, 0.4)

An understanding of the relationship between structure, particle size and magnetic properties is essential in order to design new magnetic materials. Magnetic characterizations of the samples were carried out by vibration sample magnetometer at room temperature with maximum applied field of 20kOe. Typical magnetic hysteresis loop of Three samples at temperatures 303K   is shown in figure 5. The saturation magnetization (Ms), coercivity (Hc) and remanance (Mr) of the samples are shown in table 3. The remenant ratio R=Mr /Ms shows the ease with which the direction of magnetization reorients to the nearest easy axis direction after the field is removed. The low value of R indicates the isotropic nature of the material[viii]. According to Stoner Wohlfarth model[ix], a theoretical value of Mr/Ms is 0.5 for non interacting uniaxial single domain particles with the easy axis being randomly oriented. Mr/Ms value observed is found to be 0.28 to 0.30 for three samples at room temperature which shows its isotropic nature.
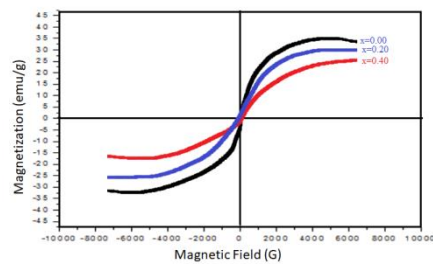
Figure 5: Hysterisis loop of $Mg_x Zn_{0.2} Ni_{0.2} Fe_{2-x} O_4$ (where x=0.0, 0.2, 0.4) at temperatures 303K

Magnetic Properties

Table 3. Saturation magnetization (Ms), coercivity (Hc) and remanance (Mr) of $Mg_x Zn_{0.2} Ni_{0.2} Fe_{2-x} O_4$ (where x=0.0, 0.2, 0.4) at temperatures 303K.

x	Composition	Saturation magnetization (Ms)in emu/gm	"Coercivity (Hc)in Oe"	"Remanance (Mr)in emu/gm"	"Mr / Ms"
0	$Mg_0 Zn_{0.2} Ni_{0.2} Fe_2 O_4$	21.34	462.5	6.38	0.30
0.02	$Mg_{0.2} Zn_{0.2} Ni_{0.2} Fe_{1.8} O_4$	26.34	495.94	7.657	0.29
0.4	$Mg_{0.4} Zn_{0.2} Ni_{0.2} Fe_{1.6} O_4$	29.45	502.14	8.347	0.28

M.S. SUBBA RAJU

CONCLUSIONS

Mg substituted Ni-Zn nanoferrites were prepared by Sol-gel method. The X-ray intensity of the (440) plane and (220) plane increases with increasing Mg^{2+} ion concentration. This shows that Mg^{2+}ions occupy both tetrahedral A site and octahedral B sites in the nano dimension. The line width Mg content. This is due to the increase in the super exchange interaction between Fe^{2+} and Fe^{3+} ions at octahedral B sites. DC electrical resistivity of the prepared samples decreases with increasing in the temperature which shows the semiconducting behaviour of nanoferrites. It is observed that the discontinuity in the figure 2 shows Curie point of the prepared ferrite samples. Curie temperature of the prepared Ni-Zn ferrites decreases with the increase of the Mg concentration. The variation of DC conductivity with temperature can be explained using the hopping mechanism of electrons between the Fe^{+2} and Fe^{+3}. The dielectric constant of the prepared ferrite samples increases with increase in temperature up to certain temperature and afterwards decreases with increase in temperature. The effect of Mg concentration on the optical properties of the nanoparticles was studied and it was observed that the absorption spectra as well as the band gap were found to be strongly dependent on nickel concentration. The optical band gap was found to decrease from 3.5 eV to 3.9 eV with the increase in Mg concentration. Thus, it can be concluded that by changing Mg concentration, the optical properties of Ni-Zn mixed ferrite nanoparticles can be tuned and hence may be optimized for applications in various fields of science and technology such as solar cell technologies, opto-electronic devices, photovoltaic and photocatalytic applications. The magnetic study reveals that the samples are ferromagnetic at room temperature.

References

[1].   Sagadevan S. Synthesis and Electrical Properties of TiO2 Nanoparticles Using a Wet Chemical Technique. American Journal of Nanoscience and Nanotechnology. 2013;1(1):27-30

[2].   E. Pervaiz and I.H. Gul, "Low temperature synthesis and enhanced electrical properties by substitution of Al^{3+} and Cr^{3+} in Co–Ni nanoferrites", Journal of Magnetism and Magnetic Materials, 343, 2013, 194-202

[3].   M.A. Gabal. "Effect of Mg substitution on the magnetic properties of NiCuZn ferrite nanoparticles prepared through a novel method using egg white", Journal of Magnetism and Magnetic Materials, vol.321, pp. 3144 – 3148, 2009

[4].   Cullity R. D., (1996), Elements of X-ray Diffraction. Addision-Wesley Public Co. INC; 42

[5].   Arulmurugan R., Jeyadevan B., Vaidyanayhan G., Sendhilnathan S., (2008), Effect of Zinc substitution on Co-Zn and Mn-Zn ferrite nanoparticles prepared by co-precipitation. *J. Magn. Magn. Mater*. 288: 470-477

[6].   Ladgaonkar B. P., Vaingainkar A. S., (1998), X-ray diffraction investigation of cation distribution in CdCu1-xFe2O4, *Mater. Chem. Phys*. 56: 280-283

[7].   W. D. Kingery, H. K. Bowen, and P. R. Uhlum, Introduction to Ceramics, Wiley, New York, NY, USA, 1975.

[8].   Shirsath S E, Toksha B G and Jadhav K M 2009 Mater. Chem. Phys. 117, 163-8

[9].   E. C. Stoner , E. P. Wohlfarth, Philos. 1948 Trans. R. Soc. A 240, 599-642